Supporting Information:

A two-dimensional lead-free hybrid perovskite semiconductor with reduced melting temperature

Akash Singh,[a,b] Ethan Crace,[a] Yi Xie,[a,b] David B. Mitzi[,a,c]*

[a]Department of Mechanical Engineering and Materials Science, Duke University, Durham, North Carolina 27708, United States

[b]University Program in Materials Science and Engineering, Duke University, Durham, North Carolina 27708, United States

[c]Department of Chemistry, Duke University, Durham, North Carolina 27708, United States

[*]Corresponding author: david.mitzi@duke.edu

Methods:

Materials:

Chemicals: 2-aminoheptane (1-methylhexylamine, 99%, Sigma Aldrich), tin (II) iodide (SnI_2, 99.999%, Thermo Scientific Chemicals), hydriodic acid (HI) solution (57 wt %, stabilized, 99.95%, Sigma Aldrich), hypophosphorous acid (H_3PO_2) solution (50 wt. % in H_2O, Sigma Aldrich), hexanes (>99%, mixture of isomers, Sigma Aldrich), paratone-N oil (Hampton Research), and diethyl ether (VWR chemicals) were procured and used without further purification. ITO-coated PEN (polyethylene naphthalate) flexible substrate was purchased from MTI corporation.

Crystal synthesis:

Crystals of $(1\text{-MeHa})_2SnI_4$ (1-MeHA = 1-methylhexylammonium) were prepared by mixing stoichiometric amounts of SnI_2 (178.8 mg, 0.48 mmol; weighed in an N_2 environment) and 2-aminoheptane (144.4 µL, 0.96 mmol) in HI (2 mL) and H_3PO_2 (0.8 mL) solution in a sealed vial at 95 °C. The hot solution was then slowly cooled to room temperature (20 °C) over a period of 80 h in a water bath, resulting in the formation of red $(1\text{-MeHa})_2SnI_4$ perovskite crystals. For comparison, crystals of $(1\text{-MeHa})_2PbI_4$ were prepared using a previously published method (Figure S1).[1]

For the single crystal X-ray diffraction (SCXRD) study, a few crystals of $(1\text{-MeHa})_2SnI_4$ were selected from the vial using a glass pipet covered in paratone-N (to restrict the crystal exposure to air). The crystals covered in oil were then quickly submerged in another reservoir of paratone-N spread over a soda-lime glass slide. Next, a suitable single crystal was identified under the optical microscope and was transferred to the SCRXD holder for measurement.

For measurements other than SCXRD, the leftover crystals from the vial were picked using a glass pipet covered in paratone-N (to restrict the crystal exposure to air) and put forth in another vial containing extra paratone-N. The new vial was then transferred into an N_2 glove box (O_2 and H_2O <0.1 ppm). Anhydrous hexane was added to the vial to dissolve the paratone-N and the resulting solution with $(1\text{-MeHa})_2SnI_4$ was filtered using a frit. The resulting crystals were further washed with hexane to remove excess paratone-N. The filtered crystals were then subsequently cleaned and washed three times using diethyl ether and stored in an N_2 glove box.

Melt-processing of films:

Melt deposition of $(1\text{-MeHa})_2SnI_4$ perovskite films was carried out using three procedures.

<u>Procedure 1</u>: A soda-lime glass substrate ($10.0 \times 10.0 \times 1.2$ mm³) was cleaned by ultrasonication in acetone, isopropyl alcohol, and deionized water for 3 min each. Upon air drying the substrate, it was transferred to an N_2-filled glove box. A few single crystals (<1.0 mg) of $(1\text{-MeHa})_2SnI_4$ perovskite were placed on the soda lime glass substrate. Crystals were then covered with an 8-µm-thick Kapton sheet and placed onto a preheated hot plate set to 160 °C (20 °C higher than the melting point to reduce viscosity and facilitate spreading); the structure was pressed on top with another preheated soda lime glass substrate (160 °C) to spread the melt. After visual inspection to ensure melting (~1 min), the overlying glass substrate was removed and the thin-film melt, sandwiched between the underlying glass substrate and overlying Kapton, was left to

crystallize by turning off the hotplate. The overlying Kapton was removed just before conducting the thin-film X-ray diffraction measurement.

<u>Procedure 2</u>: Two quartz discs (diameter = 25.4 mm and thickness = 1.5 mm, obtained from GM Associate Inc., Canada) were cleaned by ultrasonication in acetone, isopropyl alcohol, and deionized water for 3 min each. Upon air drying the substrate, they were transferred to the N_2-filled glove box, pre-annealed at 500 °C to remove any surface adsorbed moisture and were subsequently cooled back to room temperature. A few single crystals (<1.0 mg) of (1-MeHa)$_2$SnI$_4$ perovskite were placed on one of the quartz discs, which was then placed on a hotplate maintained at 160 °C. Crystals were then covered with another quartz disc preheated at 160 °C and pressed from the top to spread the melt. After visual inspection to ensure melting (~1 min), the thin-film melt, sandwiched between the two quartz discs, was left to crystallize by turning off the hotplate. After attaining room temperature (21 °C), the sample was sealed from the sides using a two-part epoxy to protect it from ambient exposure during optical absorbance, photoluminescence, and microscopic measurements.

<u>Procedure 3:</u> Two pieces of ITO coated PEN polymer substrates (10.0×27.5 mm^2, with PEN thickness of 0.125 mm and ITO thickness of 180 nm, resistivity of 12 ohm/sq) were cleaned in acetone, and IPA. Upon air drying the substrates, they were exposed under UV light for 10 minutes and finally transferred to N_2 glove box. A few single crystals (<1.0 mg) of (1-MeHa)$_2$SnI$_4$ perovskite were placed on one of the polymer substrates, which was then placed on a hotplate maintained at 160 °C. Crystals were then covered with another polymer substrate preheated at 160 °C and pressed from the top to spread the melt. After visual inspection to ensure melting (~1 min), the thin-film melt, sandwiched between the two polymer substrates, was left to crystallize by turning off the hotplate.

Single crystal X-ray diffraction:

Crystals were coated in Paratone oil, mounted on a MiTeGen loop, and transferred to a Rigaku XtaLAB Synergy equipped with a PhotonJet micro-focus x-ray source (Mo) and a HyPix 6000HE detector. Frames were collected using ω scans and the unit-cell parameters were refined against all data. An Oxford Cryostream was employed to protect the air sensitive crystals with nitrogen at all temperatures. The crystals did not show significant decay during data collection at 80 K, but the crystal did begin to grow ice on the surface. The ice on the surface of the crystal resulted in two faint powder rings at low angle, which are only prominent in the last few ω scans. Data collected at 300 K does appear to reflect some degradation—i.e., they show additional background intensity at low angle during later ω scans, coupled with a loss of some high angle diffraction peaks. Also, the structural information from SCXRD could not be obtained for the high temperature phase (i.e., above the phase transition temperature indicated by DSC, 350 K) due to poorly defined diffraction and accelerated material decomposition, resulting from exposure to small amounts of oxygen and moisture during the measurement.

Data integration, reduction, and absorption corrections were performed using CrysAlisPro 1.171.41.95a.[2] Structure solution and refinement were conducted with Olex2 version 1.5.[3] Structures are solved using olex2.solve 1.3[4] and solutions were refined against all data using SHELXL.[5] Thermal properties for all non-hydrogen atoms were refined anisotropically. Hydrogen

atoms were inserted at idealized positions and refined using a riding model with isotropic thermal parameters 1.2 times that of the attached carbon atom. Rigid bond restraints (DELU) and 1-2 and 1-3 atomic displacement parameter restraints (SIMU) were applied to the organic cation for the 300 K refinement. At this temperature there appears to be more substantial thermal motion, which introduces some disorder for the long aliphatic tail of the cation. The application of SIMU and DELU restraints stabilizes the refinement, without explicit introduction of disorder. Attempts to model the disorder (even with restraints) led to an unstable refinement.

X-ray diffraction:

The X-ray diffraction (XRD) measurement on a melt-processed film obtained through *procedure 1* (see above) was performed on a PANalytical Empyrean powder X-ray diffractometer using Cu Kα radiation, with the X-ray tube operating at 45 kV and 40 mA. The measurement was carried out over the 2θ range of 3° to 50°.

Calorimetric measurements:

Differential scanning calorimetry (DSC) measurements were performed using a TA Discovery 2500 with RCS 90 chiller. Hermetically sealed aluminum pans and lids were employed for the measurements. Prior to experiments, the DSC setup was calibrated with metallic indium (melting temperature: 156.6 °C; enthalpy of melting: 28.71 J g^{-1}), which upon repeating the experiment showed an acceptable temperature offset of 0.2 °C and melting enthalpy offset of 0.04%. Calibration and the above measurement were carried out at a ramp rate of 5 °C/min. Hermetic sealing of the pan with 1-MeHa$_2$SnI$_4$ crystals (~4 mg) was done inside the N$_2$-filled glove box to prevent exposure to ambient conditions. The sample was then subjected to three heating and cooling cycles performed at 5 °C/min in the temperature range of 20 – 160 °C. The melting temperature (T_m) was obtained from the onset of the melting endotherm. The DSC scan shown in Figure 2 represents the second scan, to allow for more effective thermal contact with the DSC pan (after melting) and to show better reversibility (See also Figure S5).

Optical absorption and photoluminescence:

Optical absorption measurements were performed on a Shimadzu UV-3600 spectrophotometer using a sampling interval of 1 nm. The absorption onset was calculated using the intersection between the onset of the UV–vis absorbance curve and the associated horizontal baseline. The photoluminescence study was carried out using an Horiba Jobin Yvon LabRam ARAMIS setup with 442 nm of wavelength excitation and using a 10% filter under a 10x objective lens. Before the measurement, the instrument was calibrated using Raman signals from a Si wafer. The obtained PL from melt-processed (1-MeHa)$_2$SnI$_4$ film is weak/noisy and therefore the raw spectrum is also smoothed (blue curve in Figure 3b of the main text) using an adjacent averaging technique.

Film morphology:

Optical microscope images of the melt-processed (1-MeHa)$_2$SnI$_4$ film (sandwiched between two quartz discs) were obtained under transmission mode using a Nikon Eclipse LV100N POL setup with 20x and 100x magnification.

Table S1. *Crystallographic data for (MeHa)₂SnI₄ at 80 and 300 K*

	80 K: (1-MeHa)₂SnI₄	300 K: (1-MeHa)₂SnI₄
Empirical Formula	$C_{14}H_{36}N_2SnI_4$	$C_{14}H_{36}N_2SnI_4$
Formula Weight, g·mol⁻¹	858.74	858.74
Temperature, K	80	300
Crystal System	Orthorhombic	Orthorhombic
Space group	*Pbca*	*Pbca*
a, Å	9.04641(16)	9.2171(4)
b, Å	8.47695(15)	8.5923(4)
c, Å	34.0759(7)	34.0460(18)
α, °	90	90
β, °	90	90
γ, °	90	90
Volume, Å³	2613.15(9)	2696.3(2)
Z	4	4
Density (calc), g·cm⁻³	2.183	2.115
Absorption coef., mm⁻¹	5.702	5.526
$F(000)$	1584.0	1584.0
Crystal size, mm³	0.135 × 0.08 ×0.009	0.293 × 0.084 ×0.009
Radiation	Mo Kα	Mo Kα
2θ range, °	4.782 to 55.744	4.786 to 52.738
Index ranges	$-11 \leq h \leq 11$ $-11 \leq k \leq 11$ $-44 \leq l \leq 44$	$-10 \leq h \leq 11$ $-10 \leq k \leq 9$ $-42 \leq l \leq 42$
Reflections collected/ Independent reflections	103955/3117	25770/2766
R_{int}, R_{sigma}	0.0741, 0.0188	0.0741, 0.0353
Data/restraints/parameters	3117/0/100	2766/58/100
Goodness-of-fit on F^2	1.478	1.357
Final R indices [$I > 2\sigma(I)$]	$R_1 = 0.0470$ w$R_2 = 0.0929$	$R_1 = 0.0843$ w$R_2 = 0.1523$
R indices (all data)[a]	$R_1 = 0.0534$ w$R_2 = 0.0944$	$R_1 = 0.1090$ w$R_2 = 0.1583$
Largest diff. peak and hole, e·Å⁻³	1.43/-1.42	1.26/-0.86

[a] $R_1 = \Sigma||F_o| - |F_c||/\Sigma|F_o|$, w$R_2 = [\Sigma w(F_o^2 - F_c^2)^2/\Sigma(F_o^2)^2]^{1/2}$

Table S2. *List of hydrogen-bonding lengths and angles of 1-MeHa$_2$PbI$_4$ (from [6]) and 1-MeHa$_2$SnI$_4$ structures at 300K. The subscripts 'eq' and 'ax' denote equatorial and axial, respectively.*

(1-MeHa)$_2$PbI$_4$			(1-MeHa)$_2$SnI$_4$		
H-bond	Length/Å	Angle/°	H-bond	Length/Å	Angle/°
N-H⋯I$_{ax}$ (1)	2.7914(4)	157.339	N-H⋯I$_{ax}$ (1)	2.8062(11)	156.263
N-H⋯I$_{ax}$ (2)	2.7762(6)	163.575	N-H⋯I$_{ax}$ (2)	2.7528(13)	163.768
N-H⋯I$_{eq}$ (3)	3.0372(10)	130.646	N-H⋯I$_{eq}$ (3)	3.0735(10)	129.783

Table S3. *List of (Sn/Pb)-I-(Sn/Pb) bond angles for interoctahedra distortions for (1-MeHa)$_2$SnI$_4$ and (1-MeHa)$_2$PbI$_4$ (from [6]) structures at 300K. The deviation of these angles from 180° reflects the magnitude of interoctahedra distortion.*

(Sn/Pb)-I-(Sn/Pb) Bond angle (°)			
(1-MeHa)$_2$SnI$_4$		(1-MeHa)$_2$PbI$_4$	
Sn-I(2)-Sn	155.727	Pb-I(2)-Pb	153.869

Table S4. *List of I-Sn/Pb-I bond lengths and bond angles for single [SnI$_6$]$^{4-}$ and [PbI$_6$]$^{4-}$ octahedra for (1-MeHa)$_2$SnI$_4$ and (1-MeHa)$_2$PbI$_4$ (from [6]) structures at 300K. These values are used to evaluate intraoctahedron distortion.*

Sn-I/Pb-I Bond length (Å)			
(1-MeHa)$_2$SnI$_4$		*(1-MeHa)$_2$PbI$_4$*	
Sn-I(1)	3.1567(10)	Pb-I(1)	3.1900(9)
Sn-I(1)	3.1567(10)	Pb-I(1)	3.1900(9)
Sn-I(2)	3.2016(10)	Pb-I(2)	3.2189(3)
Sn-I(2)	3.2016(10)	Pb-I(2)	3.2189(3)
Sn-I(2)	3.2429(10)	Pb-I(2)	3.2597(3)
Sn-I(2)	3.2429(10)	Pb-I(2)	3.2597(3)

I-Sn/Pb-I Bond angle (°)			
(1-MeHa)$_2$SnI$_4$		*(1-MeHa)$_2$PbI$_4$*	
I(2)-Sn-I(2)	86.1130	I(2)-Pb-I(2)	85.8777
I(2)-Sn-I(1)	89.9405	I(2)-Pb-I(1)	89.6258
I(2)-Sn-I(2)	93.8870	I(2)-Pb-I(2)	94.1223
I(2)-Sn-I(1)	90.0595	I(2)-Pb-I(1)	90.3742
I(2)-Sn-I(1)	86.6843	I(2)-Pb-I(1)	86.5193
I(2)-Sn-I(1)	93.3157	I(2)-Pb-I(1)	93.4807
I(2)-Sn-I(2)	93.8870	I(2)-Pb-I(2)	94.1223
I(1)-Sn-I(2)	93.3157	I(1)-Pb-I(2)	93.4807
I(1)-Sn-I(2)	90.0595	I(1)-Pb-I(2)	90.3742
I(2)-Sn-I(1)	86.6843	I(2)-Pb-I(1)	86.5193
I(2)-Sn-I(2)	86.1130	I(2)-Pb-I(2)	85.8777
I(1)-Sn-I(2)	89.9405	I(1)-Pb-I(2)	89.6258

To quantitatively evaluate the intra-octahedral distortion, we calculated the bond length distortion, $\Delta d = \left(\frac{1}{6}\right)\Sigma(d_i - d_0)^2/d_0{}^2$ (d_i are the six Sn/Pb-I bond lengths and d_0 is the mean bond length within an octahedron), and bond angle variance, $\sigma^2 = \Sigma_{i=1}^{12}(\theta_i - 90)^2/11$ (θ_i are the twelve I-Sn/Pb-I bond angles within an octahedron).[7]

2D MHP	Sn						Pb						ΔT$_m$
	T$_m$	Δd (x10^{-5})	σ^2(°^{2})	β (°)	δ (Å)	Ref	T$_m$	Δd (x10^{-5})	σ^2(°^{2})	β (°)	δ (Å)	Ref	
1-Me-HA	142.3	12.10	9.49	155.73	0.532	-/-	172.3	7.87	10.64	153.87	0.528	[6]/[6]	30.0
2-F-PEA	200.8	2.41	0.68	153.28*	0.435*	[8]/[9]	245.8	0.98*	2.71*	151.09	0.528*	[10]/[11]	45.0
PEA	213.4	6.44*	1.20*	156.51*	0.484*	[8]/[12]	252.9	3.83*	3.65*	153.08	0.571*	[10]/[7]	39.5
3-F-PEA	233.0	13.24	0.98	154.16*	0.564*	[8]/[9]	261.4	11.15	1.25	152.15	0.540*	[10]/[11]	28.4
4-F-PEA	234.2	4.68	3.81	156.38	0.564	[8]/[9]	258.9	5.80	4.29	152.94	0.552	[10]/[11]	24.7
n-BA	256.0	1.56	4.81	159.61	0.755	[13]/[13]	285.0	1.13	5.96	155.19	0.601	[13]/[13]	29.0

Table S5. *List of melting temperature (T$_m$), bond length distortion (Δd), bond angle variance (σ^2), inter-octahedra distortion angle (β), penetration depth (δ), and temperature difference (ΔT$_m$) for the common pairs of Sn- and Pb-based 2D perovskites with various organic cations. The acronym used for the organic cations are described in the parentheses as follows: 1-Me-HA (1-methyl-hexylammonium), 2-F-PEA (2-fluorophenethylammonium), PEA (phenethylammonium), 3-F-PEA (3-fluorophenethylammonium), 4-F-PEA (4-fluorophenethylammonium), and n-BA (n- butylammonium). The reference call-out is formatted as a/b where 'a' and 'b' refers to the articles from which melting temperature and structural distortion parameters are obtained respectively. Asterisk (*) represents the average values. All the reported parameters are calculated from the single crystal X-ray diffraction data collected at room temperature. The color coding is provided as a visual aid to allow for facile comparison of different structural parameters corresponding to Sn and Pb based MHPs.*

	T$_m$	Δd (x10^{-5})	σ^2(°^{2})	β (°)	δ (Å)	Electronegativity[14]
n-BA$_2$GeI$_4$	222.0	262.71	11.77	166.27	0.608	2.01
n-BA$_2$SnI$_4$	256.0	1.56	4.81	159.61	0.755	1.96
n-BA$_2$PbI$_4$	285.0	1.13	5.96	155.19	0.601	1.87

Table S6. *List of melting temperature (T$_m$), bond length distortion (Δd), bond angle variance (σ^2), inter-octahedra distortion angle (β), penetration depth (δ), and Pauling's electronegativity of (n-butylammonium)$_2$MI$_4$ where M is Ge, Sn, and Pb. All the reported parameters are calculated from the single crystal X-ray diffraction data collected at room temperature.*
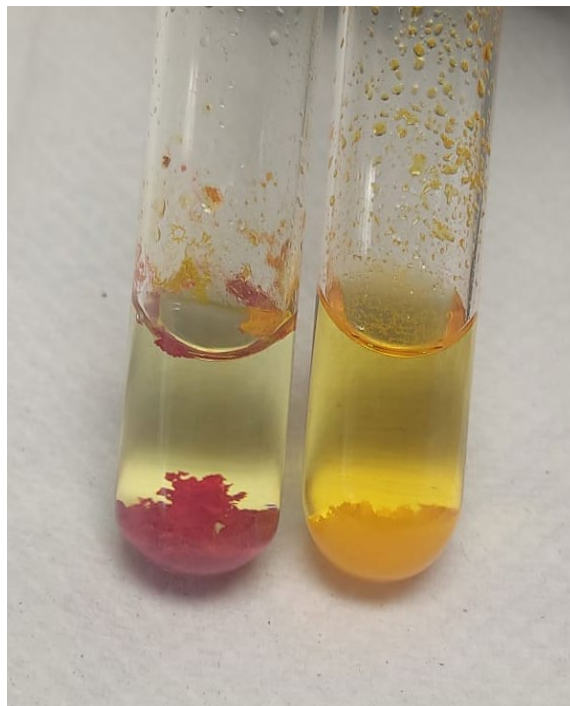
Figure S1. *Photographs of 1-MeHa₂SnI₄ (left) and 1-MeHa₂PbI₄ (right) crystals grown using the slow cooling method. The sharp distinction between the Sn- vs Pb-based crystals can be seen by their red vs yellowish appearance, respectively.*
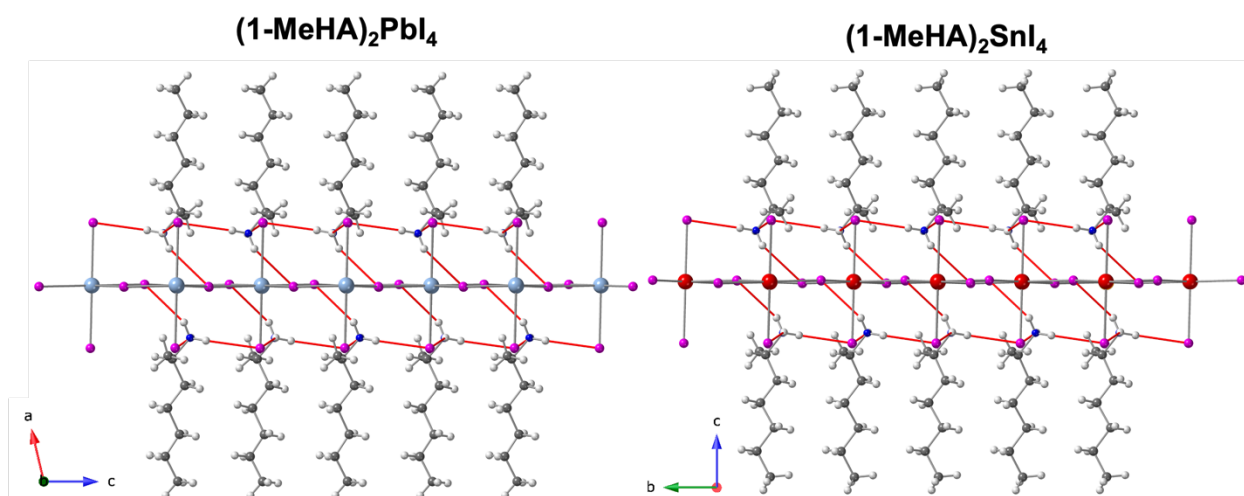
Figure S2. *Hydrogen-bonding interactions between the I atoms and 1-MeHa cations in 1-MeHa$_2$PbI$_4$ (from [6]) and 1-MeHa$_2$SnI$_4$ (current study) structures at 300K. The H-bonds are assigned according to the criterium that H$_2$N-H···I bonding distances are shorter than the van der Waals limit of 3.18 Å. Red lines denote the most significant H-bonding interactions. The "penetration depth" of the organoammonium cation into the inorganic metal-iodide cavity is calculated as the distance of the N atom below(+)/above(-) the plane of the apical iodine atoms in the inorganic sheet. Blue, red, purple, grey, dark blue, and white spheres denote Pb, Sn, I, C, N, and H atoms, respectively.*
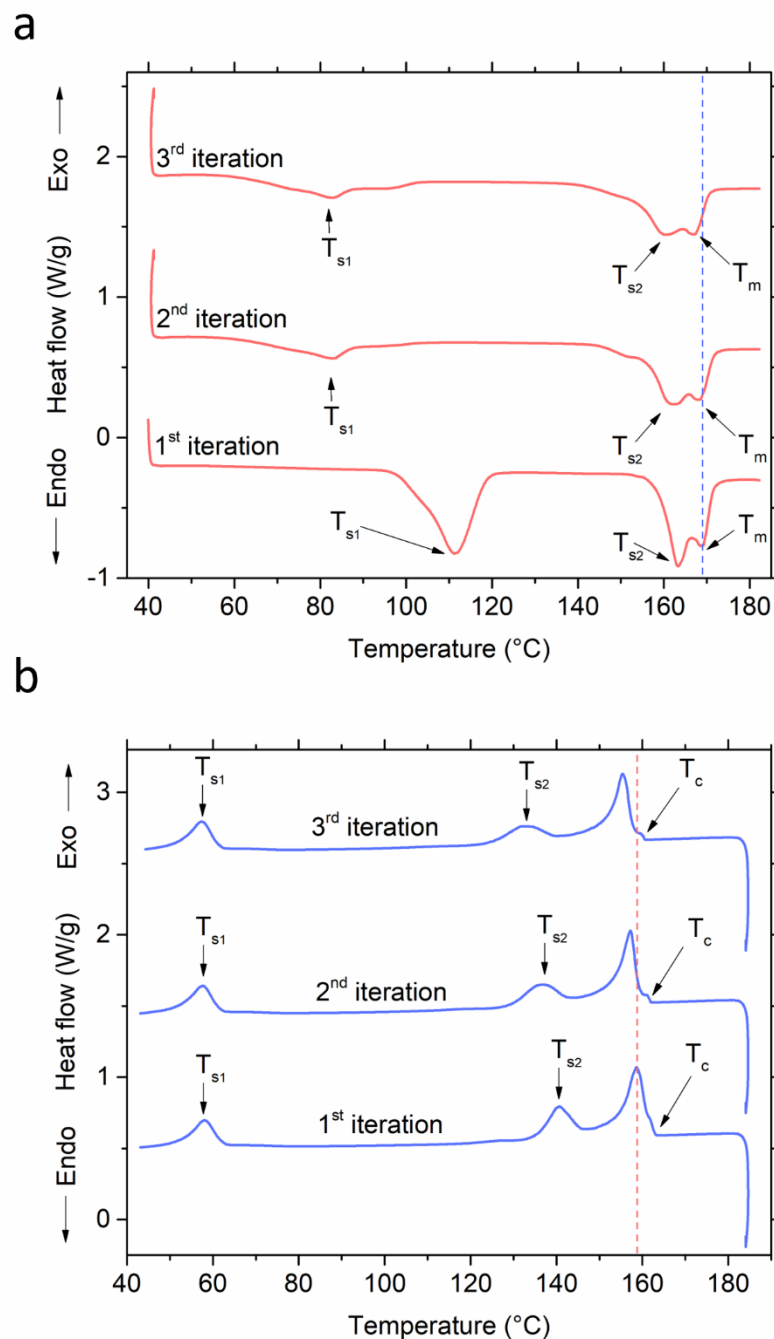
Figure S3. *Three iterations of (a) heating and (b) cooling DSC scans of 1-MeHa$_2$PbI$_4$. (a) On heating, the sample undergoes two structural transitions (T_{s1} and T_{s2}) before melting (T_m). (b) On cooling, the melted sample undergoes crystallization (T_c) before finally returning to the room temperature phase following two structural transitions. The peak of the (a) melting endotherm and (b) crystallization exotherm shifts towards lower temperatures (guided by vertical dotted line) over multiple iterations, suggesting some limited decomposition of the system under study.*
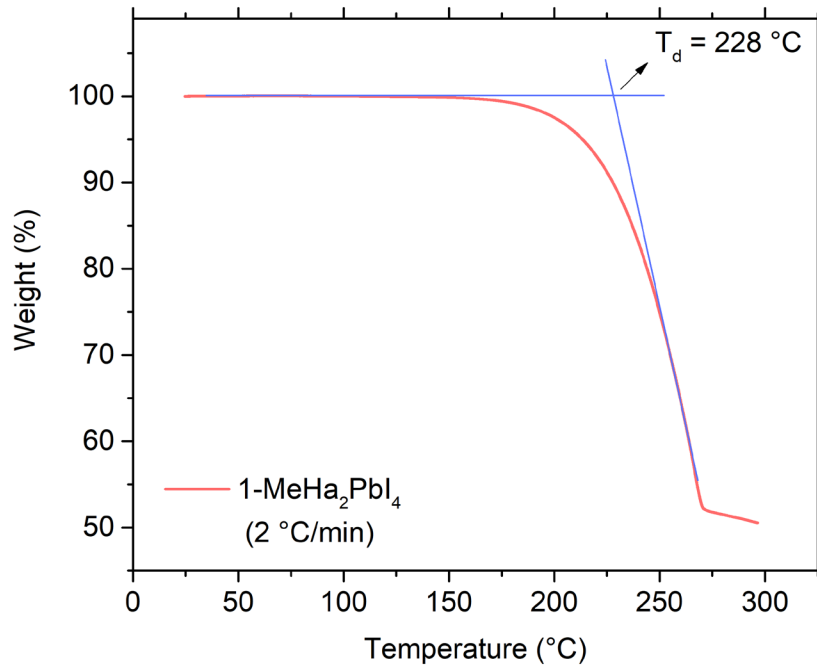
Figure S4. *Thermogravimetric analysis (TGA) of 1-MeHa₂PbI₄ showing the bulk degradation (mass loss onset) temperature (T_d = 228 °C).*
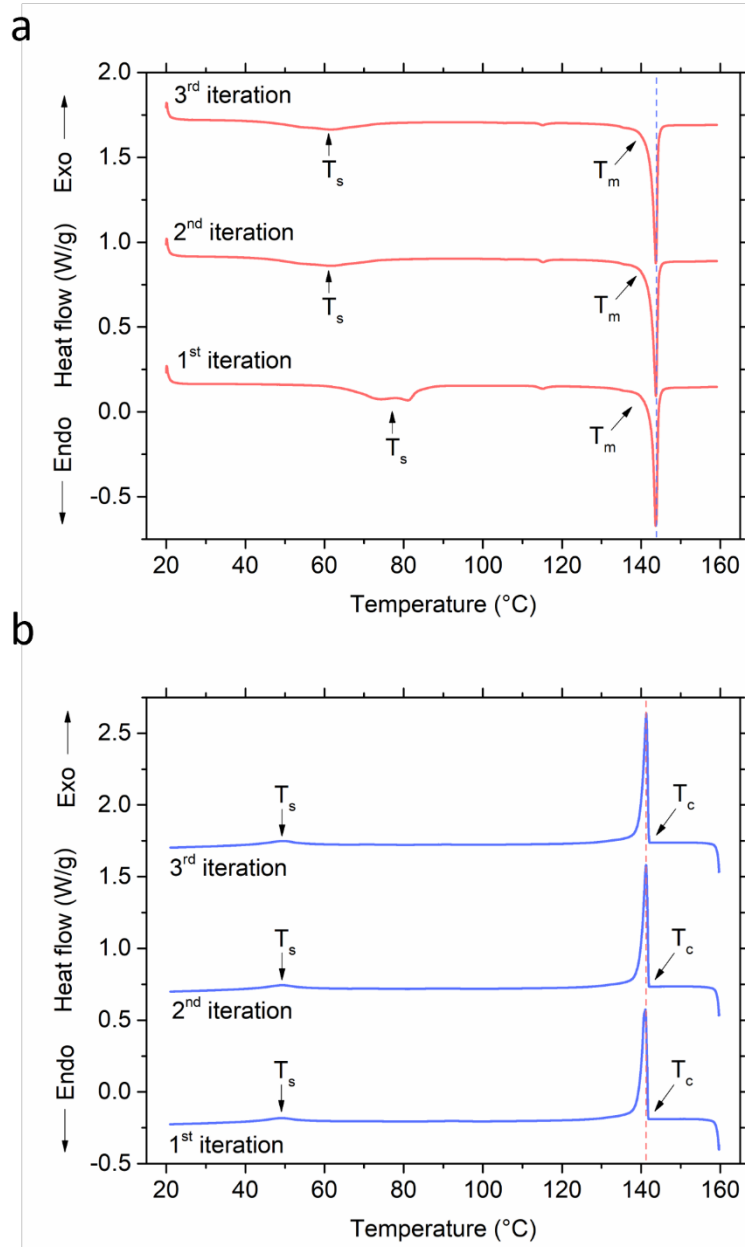
Figure S5. *Three iterations of (a) heating and (b) cooling DSC scans of 1-MeHa$_2$SnI$_4$. (a) On heating, the sample undergoes a structural transition (T$_s$) before melting (T$_m$). (b) On cooling, the melted sample undergoes crystallization (T$_c$) before finally returning to the room temperature phase following the structural transition (T$_s$). The peak of the (a) melting endotherm and (b) crystallization exotherm shows insignificant shift (guided by vertical dotted line) over multiple iterations, suggesting the stable nature of the liquified melt. The structural transition (T$_s$) during the 1st iteration is broad and right-shifted due to its sluggish nature and imperfect thermal contact between the sample and the DSC pan prior to the first melting cycle.*
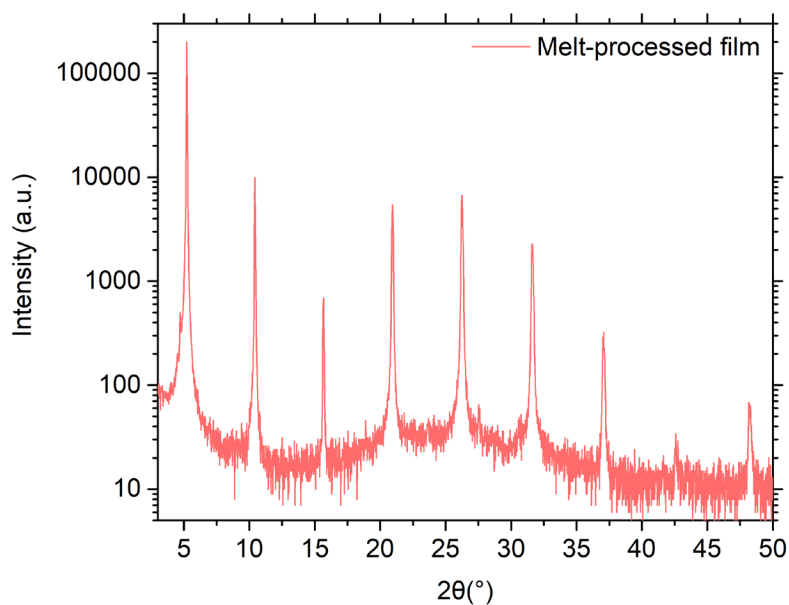
Figure S6. *X-ray diffraction pattern of melt-processed film of 1-MeHa$_2$SnI$_4$ deposited on a soda lime glass substrate (according to "Procedure 1", discussed above in Methods). The pattern resembles the typical signature of a 2D perovskite phase.*
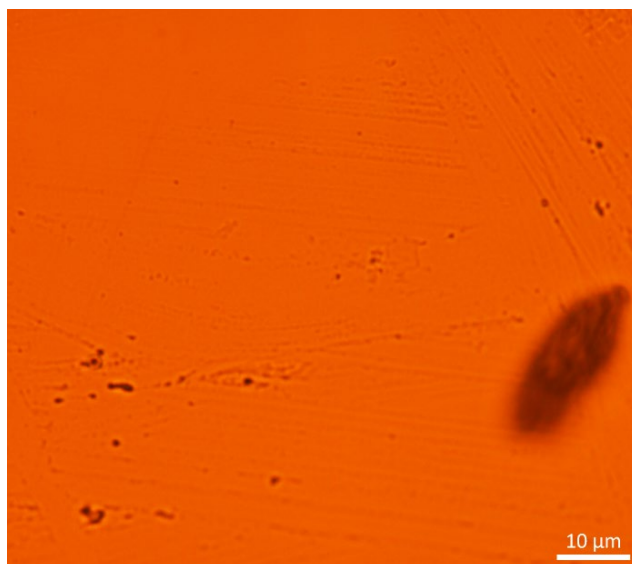

Figure S7. *Optical microscopy (under 100x magnification) of melt-processed film of 1-MeHa$_2$SnI$_4$ sandwiched between two quartz discs (deposited according to "Procedure 2", discussed above in Methods).*
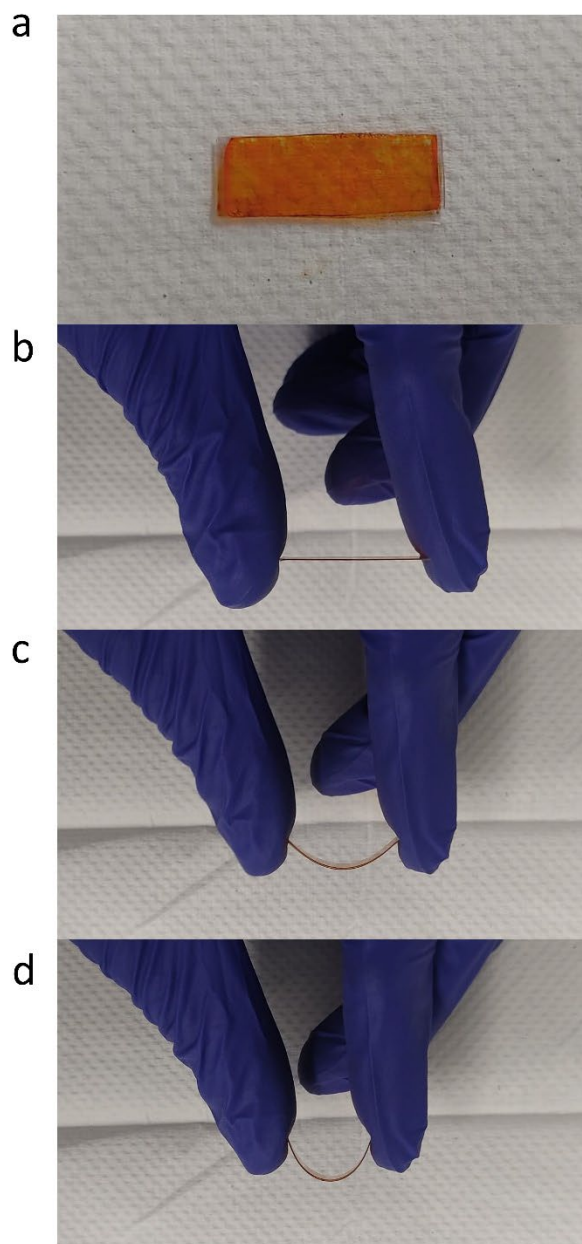
Figure S8. *(a) Photographs of melt-processed film of 1-MeHa$_2$SnI$_4$ sandwiched between two ITO-coated PEN polymer substrates (deposited according to "Procedure 3", discussed above in Methods). (b-d) The sandwiched film was bent using fingers to demonstrate its flexibility.*

References:

1. A. Singh, M. K. Jana and D. B. Mitzi, *Adv. Mater.*, 2021, **33**, 2005868.
2. Y. Rigaku OD (2021). CrysAlis PRO. Rigaku Oxford Diffraction, England.
3. O. V. Dolomanov, L. J. Bourhis, R. J. Gildea, J. A. K. Howard and H. Puschmann, *J. Appl. Crystallogr.*, 2009, **42**, 339-341.
4. L. J. Bourhis, O. V. Dolomanov, R. J. Gildea, J. A. K. Howard and H. Puschmann, *Acta Crystallogr., Sect. A*, 2015, **71**, 59-75.
5. G. Sheldrick, *Acta Crystallogr., Sect. A*, 2008, **64**, 112-122.
6. T. Li, W. A. Dunlap-Shohl, E. W. Reinheimer, P. Le Magueres and D. B. Mitzi, *Chem. Sci.*, 2019, **10**, 1168-1175.
7. K.-z. Du, Q. Tu, X. Zhang, Q. Han, J. Liu, S. Zauscher and D. B. Mitzi, *Inorg. Chem.*, 2017, **56**, 9291-9302.
8. D. B. Mitzi, C. D. Dimitrakopoulos, J. Rosner, D. R. Medeiros, Z. Xu and C. Noyan, *Adv. Mater.*, 2002, **14**, 1772-1776.
9. D. B. Mitzi, C. D. Dimitrakopoulos and L. L. Kosbar, *Chem. Mater.*, 2001, **13**, 3728-3740.
10. T. Li, W. A. Dunlap-Shohl, Q. Han and D. B. Mitzi, *Chem. Mater.*, 2017, **29**, 6200-6204.
11. J. Hu, I. W. Oswald, S. J. Stuard, M. M. Nahid, N. Zhou, O. F. Williams, Z. Guo, L. Yan, H. Hu and Z. Chen, *Nat. Commun.*, 2019, **10**, 1276.
12. V. V. Nawale, T. Sheikh and A. Nag, *J. Phys. Chem. C*, 2020, **124**, 21129-21136.
13. D. B. Mitzi, *Chem. Mater.*, 1996, **8**, 791-800.
14. D. R. Lide, *CRC Handbook of Chemistry and Physics*, CRC press, 2004.